IEEE Access
Multidisciplinary | Rapid Review | Open Access Journal

Received 7 April 2023, accepted 30 April 2023, date of publication 15 May 2023, date of current version 25 May 2023.

Digital Object Identifier 10.1109/ACCESS.2023.3276232

RESEARCH ARTICLE

Multi-Channel Colocalization Analysis and Visualization of Viral Proteins in Fluorescence Microscopy Images

CHRISTIAN RITTER[1], ROMAN THIELEMANN[1], JI-YOUNG LEE[2,3], MINH TU PHAM[2,3], RALF BARTENSCHLAGER[2,3], AND KARL ROHR[1]

[1]Biomedical Computer Vision Group, BioQuant, IPMB, Heidelberg University, 69120 Heidelberg, Germany
[2]Department of Infectious Diseases, Molecular Virology, Heidelberg University, 69120 Heidelberg, Germany
[3]German Center for Infection Research (DZIF), Heidelberg Partner Site, 69120 Heidelberg, Germany

Corresponding authors: Christian Ritter (christian.ritter@bioquant.uni-heidelberg.de) and Karl Rohr (k.rohr@uni-heidelberg.de)

This work was supported in part by the Deutsche Forschungsgemeinschaft (DFG, German Research Foundation) (SFB 1129) under Grant 240245660, and in part by the German Center for Infection Research (DZIF) under Grant 8029705712. The work of Ji-Young Lee, Minh Tu Pham, and Ralf Bartenschlager was supported in part by DZIF (TTU 05.712) under Project 8029705712; and in part by the Infectious Diseases Imaging Platform, headed by Vibor Laketa, at the CIID, Heidelberg, Germany.

ABSTRACT Automatic analysis of colocalizing biological structures in multi-channel fluorescence microscopy images is an important task to quantify and understand biological processes at high spatial-temporal resolution. Here, we introduce a software suite for colocalization analysis of spot-like objects in multi-channel fluorescence microscopy images. The software suite consists of *ColocQuant* and *ColocJ*, and is easy to use for biologists. *ColocQuant* is a Python-based software with graphical user interface to quantify colocalization of particles in two or three channels. Object-based colocalization is performed by an efficient multi-dimensional graph-based k-d-tree approach, which determines nearest neighbors involved in double or triple colocalization. *ColocJ* enables efficient and intuitive visualization of the color composition of colocalizations by a Maxwell color triangle and a color ribbon. Colocalization information can be visualized for an entire image or a selected region-of-interest. In addition, global statistics of the particle intensity, particle size, and the number of colocalizations over time are provided. The colocalization analysis results can be exported and used in other software. We illustrate the application of our software suite for multi-channel live cell fluorescence microscopy image sequences of viral proteins in hepatitis C virus infected cells. We performed two-channel and three-channel colocalization analysis.

INDEX TERMS Biomedical imaging, microscopy images, colocalization analysis, viral proteins.

I. INTRODUCTION

To gain insights into biological processes at high spatial resolution, intensive research is carried out using multi-channel fluorescence microscopy images in combination with automatic object detection and quantification. For instance, in the case of the hepatitis C virus, subcellular locations of components of the viral RNA replication machinery and virus particle components are known, but the exact subcellular site of virus assembly and the spatio-temporal coupling of viral replication to virion information remain unclear [1], [2], [3]. The location of viral proteins in the cell and their spatial relationship with subcellular structures can be assessed by colocalization analysis of fluorescently labeled proteins.

Previous work on colocalization analysis can be subdivided into intensity-based (pixel-based), object-based, and track-based approaches. *Intensity-based* approaches perform correlation analysis of the image intensities [4], [5], [6], [7], [8], [9], [10], [11], [12]. Correlation between the intensities of two-channel images can be calculated by the Pearson correlation coefficient [7] ranging from -1 to 1. However, the negative values are hard to interpret [8]. Therefore, the

The associate editor coordinating the review of this manuscript and approving it for publication was Carmelo Militello.

Manders overlap coefficient was introduced which ranges from 0 to 1 [8]. This coefficient does not consider the average intensity values of the two channels compared to the Pearson correlation coefficient. Another extension of the Pearson correlation coefficient determines a cross-correlation function by shifting one channel relative to the other channel [9]. The approach by Costes et al. [10] uses a statistical significance algorithm based on the Pearson correlation coefficient and image randomization to exclude image points with random colocalization. The approach by Li et al. [11] performs an intensity correlation analysis based on the difference of pixel intensities to the mean intensity for each channel to characterize the stained structures as segregated (different biological structures) or dependent (same biological structure). To exclude colocalizations by chance, a threshold overlap score was proposed which classifies the intensity distributions between colocalization, anti-colocalization, and non-colocalization [12]. However, intensity-based approaches are relatively sensitive to noise and use global measures for colocalization. In comparison, *object-based* colocalization approaches localize objects of interest and perform colocalization on the object level (e.g., nearest-neighbour distance). Since these approaches determine colocalization for individual objects (e.g., proteins, cells), they are more appropriate to indicate molecular interaction in order to gain insights into virus replication and assembly. Different object-based colocalization approaches have been introduced [13], [14], [15], [16], [17], [18], [19], [20]. Often, colocalization is determined by a nearest-neighbour approach which compares the positions of object centroids between two channels [13], [15], [17]. The approach of Jaskolski et al. [14] combines binary images obtained by object segmentation using a Boolean operation (disjunction) and determines colocalization within regions-of-interest (ROIs) by the difference of image intensities to the mean intensity. Statistical colocalization approaches have also been introduced which use distance-based multiple hypothesis tests [16] or exploit statistical tests to compare detected objects with objects within a ROI [19]. For 3D multi-channel microscopy images, the approach by Wörz et al. [18] uses different 3D parametric intensity models and determines colocalization based on the estimated geometry of the subcellular structures. Another colocalization approach is based on two channel 3D image cross-correlation, which is determined at each object position obtained by single-particle tracking [20]. A temporal extension of object-based colocalization are *track-based* approaches which combine spatial and temporal information [21], [22], [23]. Single-particle tracking and colocalization by trajectory correlation was used in [21]. Trajectory correlation within a window and adaptive thresholding based on the Pearson correlation coefficient was also employed [22]. In addition, a probabilistic tracking approach with integrated colocalization analysis was introduced [23]. This approach is based on a combination of the Kalman filter and particle filter for tracking, and jointly performs tracking and colocalization analysis. However, the track-based colocalization approaches described above determine colocalization only based on two-channel fluorescence microscopy images. To gain further insights into virus assembly, more than two fluorophores could be used for labelling structures of interest and therefore colocalization needs to be determined in multi-channel fluorescence microscopy images with more than two channels.

Different publicly available plugins and software suites for colocalization analysis for different types of image structures (e.g., cells, spot-like structures) are available to support biologists in image analysis, such as JACoP v2.0 [4], Squassh [24], DiAna [25], EzColocalization [26], and Colocalization Colormap [27]. Further, the ImageJ [28] platform provides plugins such as Coloc 2, Colocalization Finder, and ComDet. Intensity-based colocalization analysis can be performed with JACoP v2.0, Squassh, EzColocalization, Coloc 2, and Colocalization Finder. Object-based colocalization can be performed by JACoP v2.0, Squassh, DiAna, Colocalization Colormap, and ComDet. The ImageJ plugins JACoP v2.0, Squassh, DiAna, Colocalization Colormap, Coloc 2, and Colocalization Finder determine colocalization in two-channel images. EzColocalization and ComDet are able to analyse images with more than two channels. However, both software do not provide a visualization of the color distribution of colocalized objects (e.g., Maxwell color triangle), and do not use an efficient multi-dimensional graph-based approach to compute colocalizations. In addition, EzColocalization was designed for cells and is not suited for spot-like structures. Existing publicly available software do not provide a quantification and visualization of the color distribution and spatial distribution for each colocalized object.

In this work, we introduce a software suite for object-based detection, quantification, and visualizations of colocalizations of spot-like subcellular structures in multi-channel fluorescence microscopy images. The Python-based software *ColocQuant* enables to detect and colocalize spot-like structures (particles) in two-channel and three-channel fluorescence microscopy images. Colocalization is determined based on an efficient multi-dimensional graph-based k-d-tree approach to identify colocalized particles between two channels (double colocalization) or three channels (triple colocalization). In addition, colocalization parameters are quantified such as object position, object intensity, and object size for each channel and each colocalized object. Double and triple colocalized objects can be visualized by *ColocJ*. We are the first that propose an efficient and intuitive visualization of the color composition of colocalizations by a Maxwell color triangle (triple colocalization) and a color ribbon (double colocalization). Further, the spatial distribution of a triple colocalization is visualized by a triangle representing the location and distances of involved particles. The developed visualization techniques can be used for inspection of acquired fluorescence microscopy image sequences, for example, to identify and assess abnormal intensity changes

over time (e.g., due to imaging or staining artifacts). Global statistics of the object intensity, object size, and number of colocalizations over time are provided as box plots, bar plots, or tables, and can be exported and used in other software for further analysis. ColocJ can be used for an entire image or for a manually selected ROI annotated with ImageJ built-in tools. The software can be applied for static and dynamic image data. Our software suite consists of two software tools to have a modular design and to increase the flexibility, both for users from biology and for software developers (e.g., combination with other software). We illustrate the application of ColocQuant and ColocJ on data of multi-channel live cell microscopy images of hepatitis C virus (HCV) encoded proteins. We performed colocalization in two as well as in three channels. Further, we demonstrate the visualization of the spatial distribution for triple colocalization and the color composition analysis for double and triple colocalization.

II. METHODS

A. QUANTIFICATION OF COLOCALIZATION USING ColocQuant

We developed *ColocQuant*, a Python-based software which uses an efficient multi-dimensional graph-based approach to determine colocalized objects in two-channel (double colocalization) or three-channel (triple colocalization) fluorescence microscopy images. We use a k-d-tree [29] to perform a nearest neighbor search over two or three channels. In our approach, a triple colocalized particle is represented by a vector $\mathbf{v}_{\text{triple}} = (\mathbf{p}_1, \mathbf{p}_2, \mathbf{p}_3)^T$ which contains position vectors $\mathbf{p}_i = (x_i, y_i)^T$ for each channel i. $\mathbf{p}_i$ represents the position of a particle (viral structure) in channel i which is detected by the spot-enhancing filter (SEF) [30]. Particle detection by SEF consists of applying a Laplacian-of-Gaussian (LoG) filter with standard deviation $\sigma_{\text{LoG},i}$ (filter size), followed by thresholding the filtered image using the mean intensity plus a factor c_i times the standard deviation (detection threshold). After particle detection, a k-d-tree for all particle positions $\mathbf{p}_i \in \mathbb{R}^k$ with $k = 2$ of channel i is constructed which is a binary tree in which each non-leaf node represents a splitting hyperplane that divides the search space into two parts. The root node $\mathbf{p}_{\text{root}}$ of the tree splits all points $\mathbf{p}_i$ into two subspaces according to one of the dimensions (x_i or y_i). The hyperplane is perpendicular to the chosen dimension (x_{root} or y_{root}) and all points $\mathbf{p}_i$ with $\{(x_i, y_i)|x_i < x_{\text{root}}\}$ (or $\{(x_i, y_i)|y_i < y_{\text{root}}\}$ for splitting along the y-dimension) are represented by the left subtree, whereas the remaining points are represented by the right subtree. Afterwards, the subtrees are split in a similar fashion and along alternating dimensions of $\mathbf{p}_i$. Once the k-d-tree is build, a nearest neighbor query between a point $\mathbf{p}_i$ in channel i and points $\mathbf{p}_j$ in channel j is defined by $\{(\mathbf{p}_{j,1} \neq \mathbf{p}_{j,2}) \Rightarrow [D(\mathbf{p}_i, \mathbf{p}_{j,2}) \geq D(\mathbf{p}_i, \mathbf{p}_{j,1})]\}$, where $D(\cdot)$ is the Euclidean distance and $\mathbf{p}_{j,1}$ is the nearest neighbor of $\mathbf{p}_i$, and $\mathbf{p}_{j,2}$ is the second nearest neighbor. We assume that the nearest neighbor is within a distance $D(\mathbf{p}_i, \mathbf{p}_{j,1}) \leq D_{\max,i,j}$, which can be chosen in the GUI of ColocQuant by the user. The construction of a k-d-tree and the representative search space for querying the k-d-tree to determine the nearest neighbor is illustrated in Fig. 1.

To detect double colocalized objects $\mathbf{v}_{\text{double}} = (\mathbf{p}_1, \mathbf{p}_2)^T$, the k-d-tree of channel 1 needs to be queried only once with points from channel 2 using $D_{\max,1,2}$. For a triple colocalization, the k-d-tree of channel 1 needs to be queried by channel 2 (with $D_{\max,1,2}$) and 3 (with $D_{\max,1,3}$) as well as a second k-d-tree needs to be build based on points from channel 2 and queried by channel 3 (with $D_{\max,2,3}$). Afterwards, the intersection of all nearest neighbor queries is computed, which determines triple colocalizations within all three channels. Due to the data structure of k-d-trees, the nearest neighbor queries have an average running time of $\mathcal{O}(\log(n))$, where n is the number of particles in a channel [29], [31], [32]. Thus, this data structure is efficient, easy to construct, and well suited for finding nearest neighbors to determine triple colocalizations.

B. VISUALIZATION OF COLOCALIZATION USING ColocJ

Besides the spatial information of double or triple colocalized objects (e.g., position, size) determined by ColocQuant, fluorescence intensity information in each of the channels is important. We developed *ColocJ*, an ImageJ macro, to visualize the color distribution and composition of double as well as triple colocalization. We are the first that propose an efficient and intuitive visualization of the color composition of colocalizations of spot-like structures by a Maxwell color triangle (triple colocalization) and a color ribbon (double colocalization). Generally, each color intensity c can be represented by a weighted mixture of the primary colors within the trichromatic RGB space representation (R=red, G=green, B=blue) [33], [34] with $c = e\,R + f\,G + g\,B$, where e, f, g are factors in the interval [0, 1], and the primary colors can be visualized. For a better and easier comparison of the color composition of double and triple colocalized objects, we suggest visualizing the proportions of the three primary colors. For double colocalized objects, a color ribbon showing a color gradient between two colors is used to visualize the proportion of both color values. For a triple colocalized object, the Maxwell color triangle is proposed to visualize the proportion of the three primary colors. The Maxwell color triangle consists of three coordinate axes, one for each color, which are the altitudes of the triangle ranging from zero (foot) to one (vertex of the triangle). The value of each primary color expresses its intensity compared to the intensity of the other two primary colors. To represent an RGB color value in the triangle, the RGB color values need to be normalized by multiplying with a factor a such that $a\,R + a\,G + a\,B = 1$ is fulfilled. The factor a is based on the sum of the primary color values with $a = 1/(R + G + B)$. As an example, the Maxwell color triangle value of the 8-bit RGB color red with (R=255, G=0, B=0) is ($\text{R}_{\text{Maxwell}} = 1$, $\text{G}_{\text{Maxwell}} = 0$, $\text{B}_{\text{Maxwell}} = 0$) with $a = 1/255$ and located at the red vertex of the triangle. The 8-bit RGB color white (R=255, G=255, B=255) is multiplied by

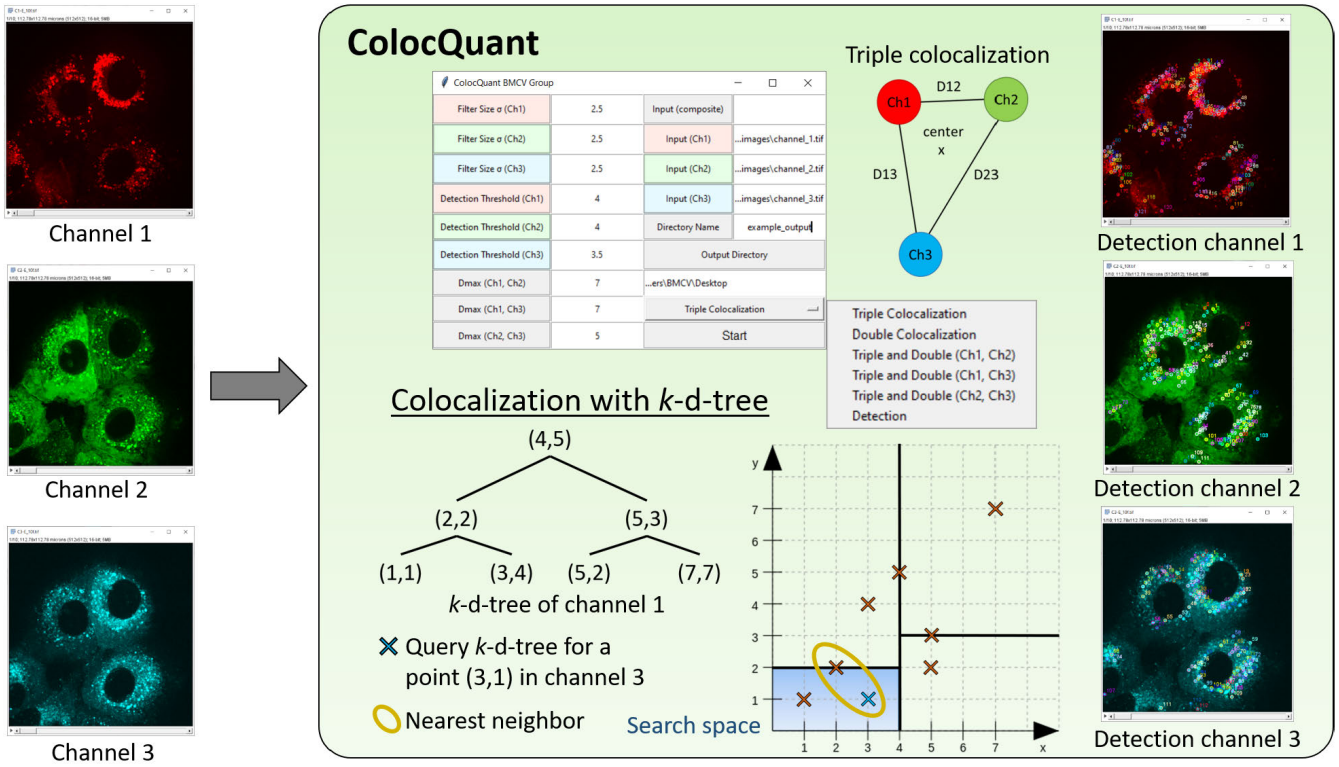

FIGURE 1. Overview of ColocQuant.

$a = 1/(255 + 255 + 255)$ and located at the center of the Maxwell color triangle. Note that, for example, the 8-bit RGB color (R=5, G=5, B=5) is multiplied with $a = 1/(5+5+5)$ and therefore also located at the center of the Maxwell color triangle. This is due to the fact that the Maxwell color triangle quantifies and visualizes the proportion of the three primary colors to each other. Therefore, the Maxwell color triangle provides additional object-based color information compared to the intensity box plots, which provide single channel global intensity statistics.

The computation of the color composition for double and triple colocalization is illustrated in Fig. 2. A double colocalization is marked by a yellow circle in the composite image. The image intensities are extracted at the center of the double colocalization (center of yellow circle) for each channel and the ratio between the two intensities is computed. In addition, image intensities can also be extracted at the position of the detected particle in each channel. The intensity ratio determines the position on the color ribbon and represents the color composition of the double colocalization. In Fig. 2 the color composition analysis is exemplarily shown for channel 1 and 2. Note that ColocJ also provides the possibility to analyse the color composition for colocalization of channel 2 with 3 as well as channel 1 with 3. A triple colocalization is marked with a yellow circle in the composite image whereas the yellow triangle vertices represent the position of detected particles in each of the three channels. The intensity information for each channel can be extracted at the center of the yellow circle representing the overlap region of the colocalization or at the position of the detected particle in each channel. Based on the extracted intensity values, the ratio for each primary color is determined and the color composition of a triple colocalization is marked with a black dot in the Maxwell color triangle.

III. RESULTS

We applied *ColocQuant* and *ColocJ* using live cell fluorescence microscopy images displaying different hepatitis C virus (HCV) proteins expressed in virus-replicating cells. The image data consists of a three-channel time-lapse image sequence displaying HCV-infected cells with mCherry-labeled host cell protein apolipoprotein E (ApoE) (channel 1), GFP-labeled HCV envelope glycoprotein E2 (channel 2), and mTurquoise-labeled HCV non-structural protein 5A (NS5A) (channel 3) within Huh7/LunetCD81H cells [2]. The image sequence comprises 10 images with an image size of 512 × 512 pixels and a spatial resolution of 220 nm/pixel. Images were acquired with a PerkinElmer UltraVIEW ERS spinning disk confocal microscope mounted on a Nikon TE2000-E.

With the GUI of ColocQuant (see Fig. 1), we parameterized SEF for particle detection with a *filter size* (LoG standard deviation $\sigma_{\mathrm{LoG},i}$) of 2.5 for all three channels. The *detection threshold factor* c_i was set to 4.0 for channel 1

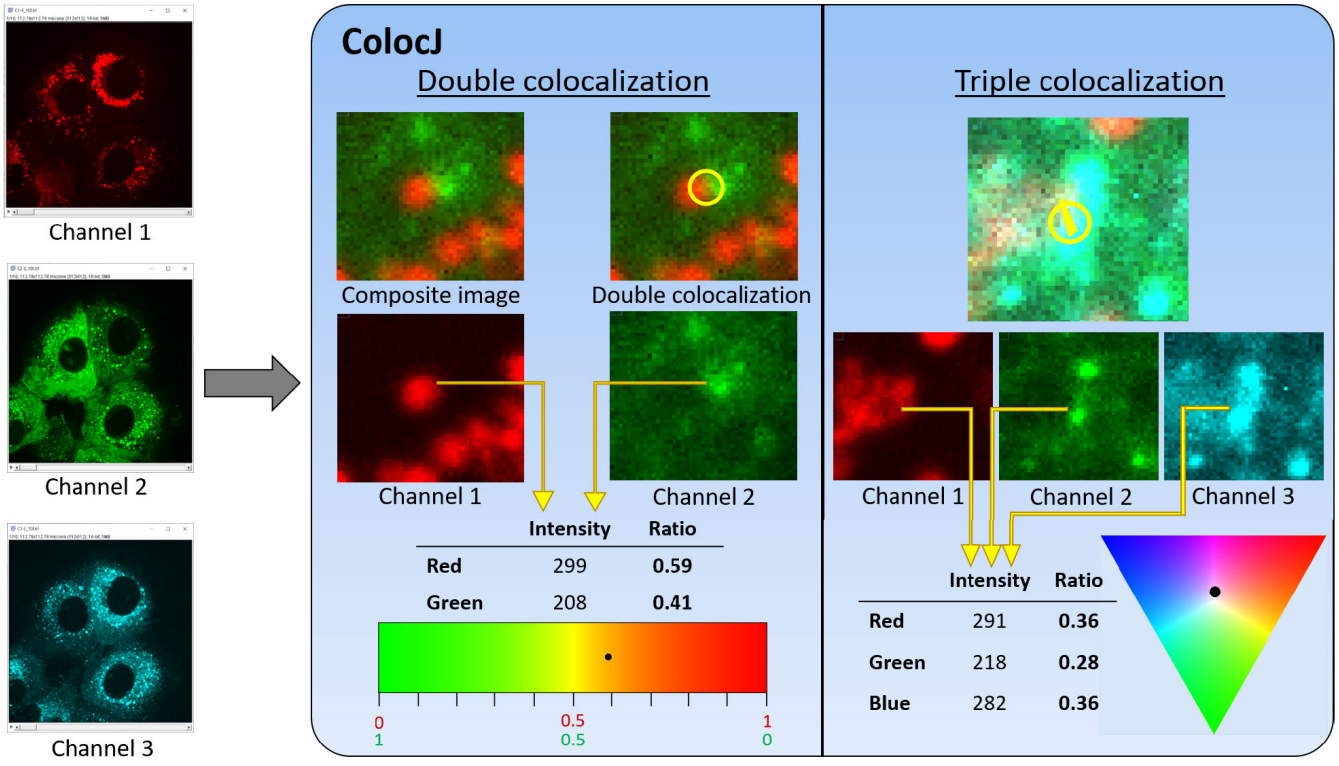

FIGURE 2. Overview of ColocJ.

and 2, and to 3.5 for channel 3. To determine triple colocalizations, the maximum Euclidean distance between detections in the different channels was set to 7 for $D_{max}(Ch1,Ch2)$ and $D_{max}(Ch1,Ch3)$, and 5 for $D_{max}(Ch2,Ch3)$. We used different parameter values because ApoE (channel 1) showed a higher motility compared to E2 and NS5A.

After identifying triple colocalizations for each frame of an image sequence, the determined objects can be visualized by *ColocJ*. The visualization of the spatial composition for a triple colocalization is shown in Fig. 3. A yellow circle is used to visualize the position where a triple colocalization occurs. The triangle vertices indicate the location of the detected particles of the triple colocalization in each channel and the edges provide information about the distances. The analysis and visualization of the spatial composition of triple colocalizations can be performed for composite images (overlay of all channels) and for each channel separately.

The color composition and statistical analysis of triple colocalizations by ColocJ is shown in Fig. 4. ColocJ provides a bar plot showing the number of colocalizations in each frame and allows the user to analyze the number of triple colocalizations over time. This parameter is important to study the temporal behavior of the assembly process. In addition, ColocJ visualizes the distribution of the size of particles for each channel that are involved in a triple colocalization. The size is determined by counting the pixels that belong to the connected component [35] representing the detected particle by SEF. Based on the object sizes, fluorescence labelling can be assessed, viral proteins can be characterized, and differences between channels can be determined. For the considered HCV image sequence, all three channels show a similar object size for each channel and the number of colocalizations is nearly constant over time. To analyse the intensity distribution of triple colocalizations, ColocJ provides box plots of the intensity values for each channel as well as a visualization by the Maxwell color triangle. The box plots visualize global statistics of the absolute intensity values independently of the remaining two channels. In comparison, the Maxwell color triangle represents the proportion of intensity values between the three channels for each triple colocalization and provides an object-based statistical visualization. Therefore, the two visualization approaches display different aspects of a triple colocalization and complement each other. In addition, ColocJ provides the possibility to extract the intensity information for the Maxwell color triangle at the center of the triple colocalization (center of the yellow circle shown in Fig. 3) as well as at the positions of the yellow triangle vertices. Comparing both types of Maxwell color triangles for the HCV image sequence, it turns out that using the center of the triple colocalization is more heterogeneous (larger spread of the black dots) than using the positions of the triangle vertices. To analyse the image data at the single-cell level, ColocJ provides the possibility to visualize triple colocalizations for a manually selected ROI (see Fig. 4). The

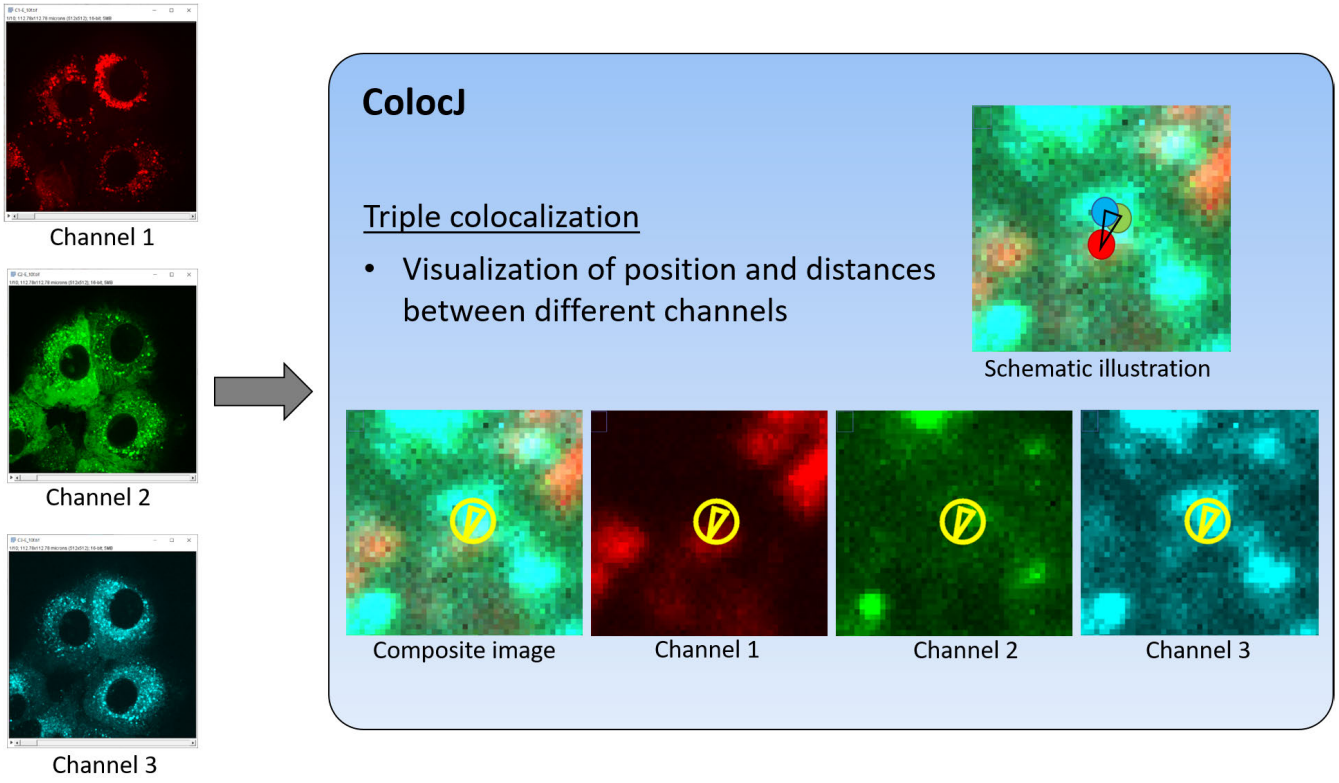

FIGURE 3. **Visualization of spatial composition for triple colocalization using ColocJ.**

ROI can easily be determined by the ImageJ built-in area selection tool *Polygon* and imported to ColocJ. All visualized data of the colocalization analysis by ColocJ is also provided in a table format shown in Fig. 5. The table can be saved as a *CSV* (comma-separated values) file in ImageJ and therefore, can easily be imported and exploited by other software.

Besides analyzing triple colocalizations, ColocQuant and ColocJ can also be used to analyze double colocalizations of two-channel fluorescence microscopy images. Based on the selected channels, ColocJ visualizes the number of double colocalizations as a bar plot shown in Fig. 6. As for triple colocalizations, ColocJ also displays statistics about the object size as box plots. The color distribution of double colocalizations can be analysed by intensity box plots showing statistics of the absolute intensity values, and the color composition can be analysed with a color ribbon for object-based analysis. In Fig. 6 the three-channel HCV image sequence is used for double colocalization between channel 1 and 2 as an example. Note that, ColocQuant and ColocJ can visualize all combinations of channels selected by the user as indicated by the different color ribbons in Fig. 6. To quantify the performance of our software, we manually determined the number of colocalizations between channel 1 and 2 as ground truth for the HCV live cell image sequence within a region-of-interest for three time points (frames 1, 5, 10). As performance measures we computed the Precision P, Recall R, and $F1$ score. We obtained mean values of P= 86%, R=82%, and $F1$=79%. The result is promising for the considered challenging image data (highly heterogeneous image structures, strong fluorescence signal of other image structures besides the spot-like structures, and strong image noise). We also performed a comparison with an existing software as a control experiment. We applied the ImageJ plugin JACoP v2.0 for double colocalization analysis between channel 1 and 2 of the HCV live cell image sequence comprising ten time points (Fig. 7). It turned out that the obtained number of colocalizations at different time points agrees well with that of ColocQuant/ColocJ in Fig. 6. Note that applying JACoP v2.0 to image sequences is tedious since each frame of the sequence needs to be separately loaded, parametrized, and processed. In contrast, our software allows analyzing all frames of the image sequence at once. In addition, our software suite can quantify double colocalizations for a manually selected ROI. As for triple colocalizations, the user can import a selected ROI. ColocJ provides all double colocalization statistics (e.g., location, intensity, size of particles involved in double colocalization) as a table format for exporting and further processing with other software.

A. MAXWELL COLOR TRIANGLE TO ASSESS IMAGE INTENSITY CHANGES

The developed visualization techniques can be used to inspect acquired microscopy image sequences, for example, to identify and assess abnormal intensity changes over time

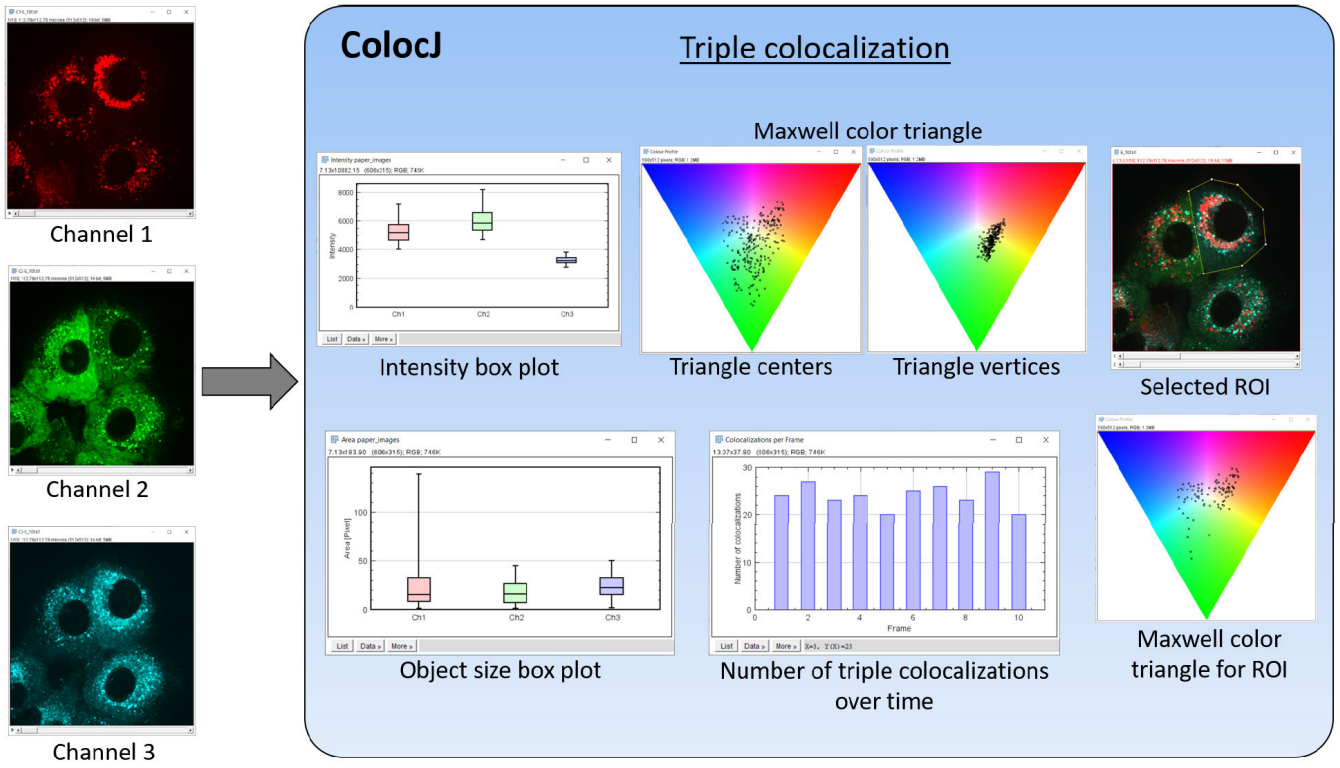

FIGURE 4. Triple colocalization analysis of HCV live cell image sequence using ColocJ.

Results

File Edit Font Results

	number	X_mean	Y_mean	frame	X_ch1	Y_ch1	Intensity_ch1	Area_ch1	X_ch2	Y_ch2	Intensity_ch2	Area_ch2	X_ch3	Y_ch3	Intensity_ch3	Area_ch3
1	1	143.8683	132.2042	1	145.8777	134.6768	4930.7857	11	143.3446	131.1552	6616.0291	34	142.3828	130.7808	3074.8972	16
2	2	161.6578	125.011	1	164.1444	121.9458	4887.3146	29	161.9014	126.9156	4644.402	37	158.9277	126.1715	2784.9698	15
3	3	169.2292	263.3473	1	169.877	264.3349	4664.3629	9	169.4905	262.9389	5959.2051	27	168.3201	262.7682	2758.9361	12
4	4	170.6658	135.7957	1	167.4618	132.8855	5371.8535	49	172.6493	137.3679	6315.8106	26	171.8864	137.1337	3222.2569	8
5	5	173.5404	150.8256	1	174.3915	146.4532	5879.7969	34	173.6524	152.9839	7955.0118	42	172.5773	153.0396	3184.1629	30
6	6	192.4086	154.1666	1	191.4752	149.6876	5358.1788	17	193.584	156.331	6724.1519	26	192.1668	156.4813	3340.6276	10
7	7	241.1697	148.0253	1	240.945	149.462	5079.4983	32	242.0556	146.9313	5365.0705	5	240.5087	147.6826	3237.0314	29

FIGURE 5. Results of triple colocalization analysis by ColocJ for a live cell HCV image sequence. The table provides information about the number of colocalizations, location, frame number, intensity, and size of the particles involved in a triple colocalization.

(e.g., due to imaging or staining artifacts). We studied the visualization based on the Maxwell color triangle in *ColocJ* for different typical intensity changes occurring in multi-channel fluorescence microscopy images. Intensity variations can be separated in linear and non-linear changes. A *linear* intensity change over time means that the intensity values linearly increase or decrease. Such a change can occur for labeled virus associated proteins, for example, due to virus-host cell interactions [20], [36], [37]. A *non-linear* intensity change over time means that the intensity values non-linearly increase or decrease over time. An example is photobleaching in fluorescence microscopy, where the number of fluorescent molecules is reduced due to permanent photochemical destruction which leads to an exponential (non-linear) intensity decrease over time [38], [39].

We studied the visualization based on the Maxwell color triangle using a three-channel live cell fluorescence microscopy image sequence consisting of 10 frames with an image size of 1114 × 1496 pixels and a spatial resolution of 89 nm/pixel. The image data displays HCV-infected cells with mCherry-labeled host cell protein ApoE (channel 1), YFP-labeled HCV protein E2 (channel 2), and mTurquoise-labeled HCV protein NS5A (channel 3) [2]. Images were acquired with a PerkinElmer UltraVIEW VoX spinning disk confocal microscope mounted on a Nikon TiE.

We first considered the case where the intensity values of channel 1 (ApoE, red color) linearly decrease over time. We simulated this change by decreasing the original intensity values by a factor of 20 times the time point t (e.g., for $t = 9$ all intensity values of channel 1 are decreased by

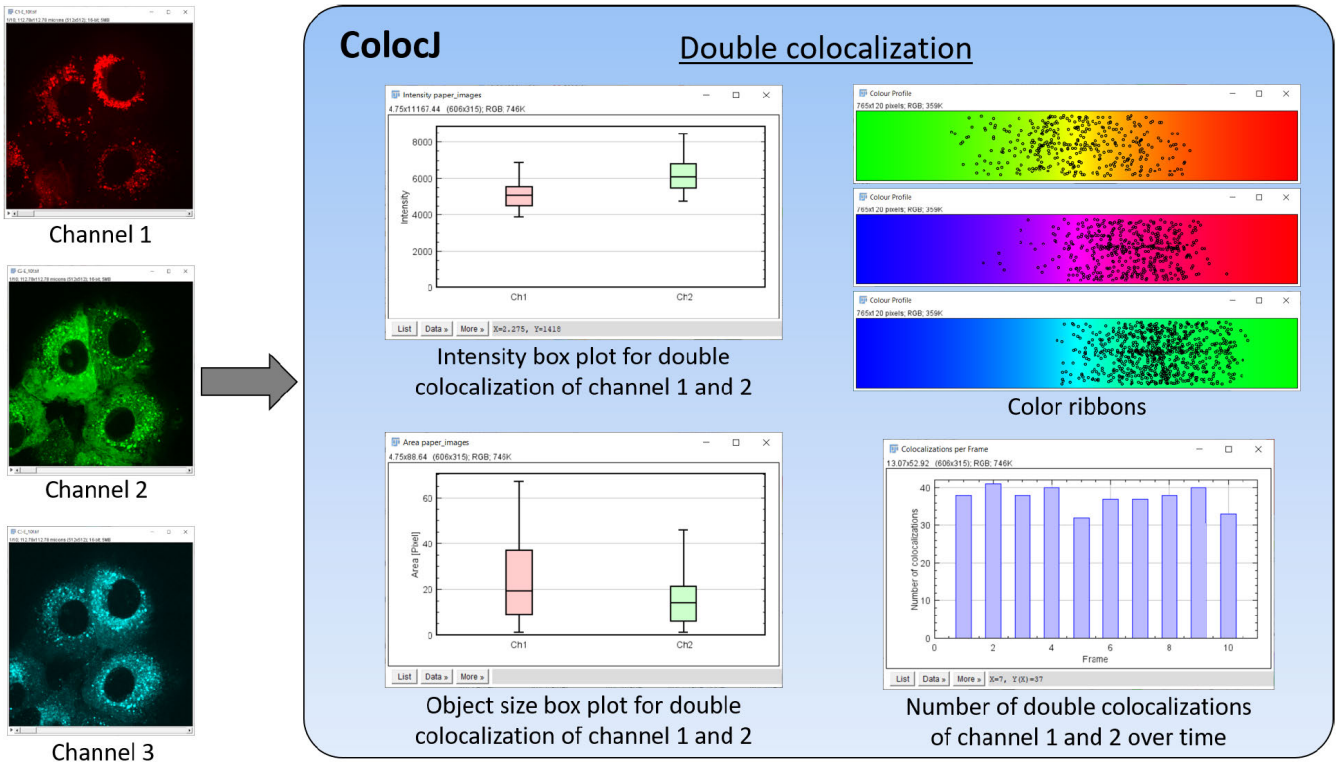

FIGURE 6. Double colocalization analysis of HCV live cell image sequence with ColocJ.

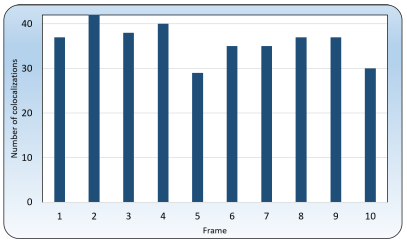

FIGURE 7. Number of double colocalizations of channel 1 and 2 for HCV live cell image sequence with JACoP.

180). The intensity values of channel 2 (E2) and channel 3 (NS5A) remain unchanged. Fig. 8 shows the original composite images for different time points as well as the composite images with decreasing channel 1 intensity values. Fig. 9 shows the Maxwell color triangle for both image sequences. The black dots represent the same triple colocalizations. It can be seen that the black dots for the image sequence with decreasing intensity values in channel 1 shift towards the blue/green color region for progressing time points since the red color is decreased. For time point $t = 0$, both Maxwell color triangles are equal since the intensity values for channel 1 are equal for both image sequences.

We also considered the case when the intensity values of *all* three channels are linearly increasing over time (using the same constant factor as in the example above). Fig. 10 shows the Maxwell color triangle for the original image sequence as well as for the image sequence with increasing intensity values in all three channels. The black dots for both image sequences represent the same triple colocalizations to facilitate a comparison. It can be seen that the distribution of the black dots is similar. It can also be observed that the black dots of the image sequence with increasing intensity values shift towards the center of the Maxwell color triangle over time. This effect can also be proofed mathematically. We show this in the Appendix together with other proofs for linear and non-linear intensity changes in a single channel and in all channels. Biological findings derived using our software are described elsewhere [40].

IV. DISCUSSION

We introduced a software suite consisting of *ColocQuant* and *ColocJ* to analyze, quantify, and visualize colocalization of spot-like structures such as viral proteins in multi-channel fluorescence microscopy image sequences, which can be applied both for whole images and for single cells based on selected regions-of-interest. The software has several advantages compared to existing colocalization analysis software such as object-based identification of triple colocalization and color composition analysis. *ColocQuant* uses an efficient approach based on k-d-trees to identify particles in different channels that are involved in double or triple colocalization. *ColocJ* provides an efficient and

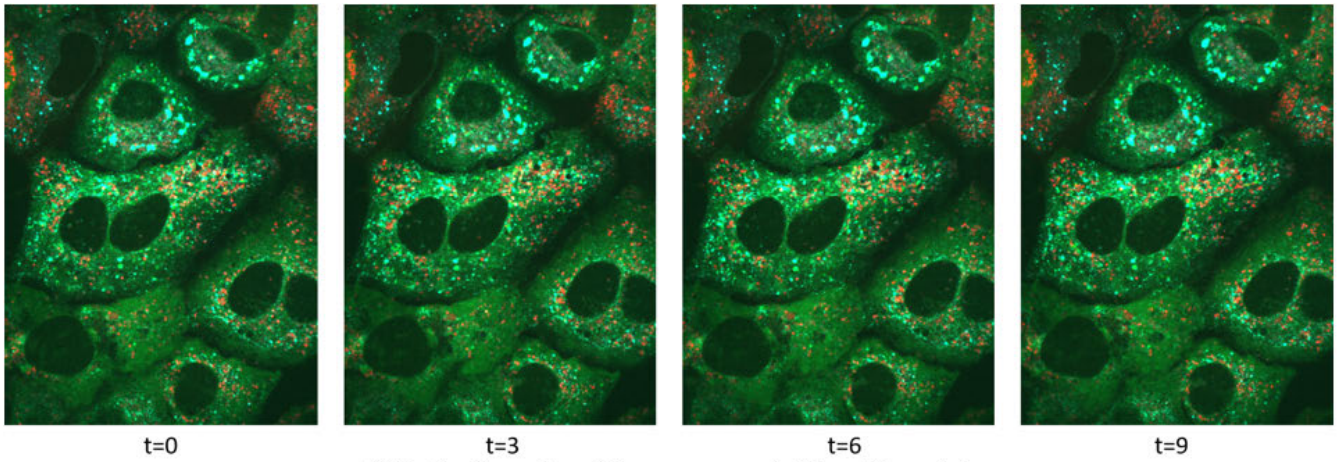

(a) Original three-channel image sequence at different time points.

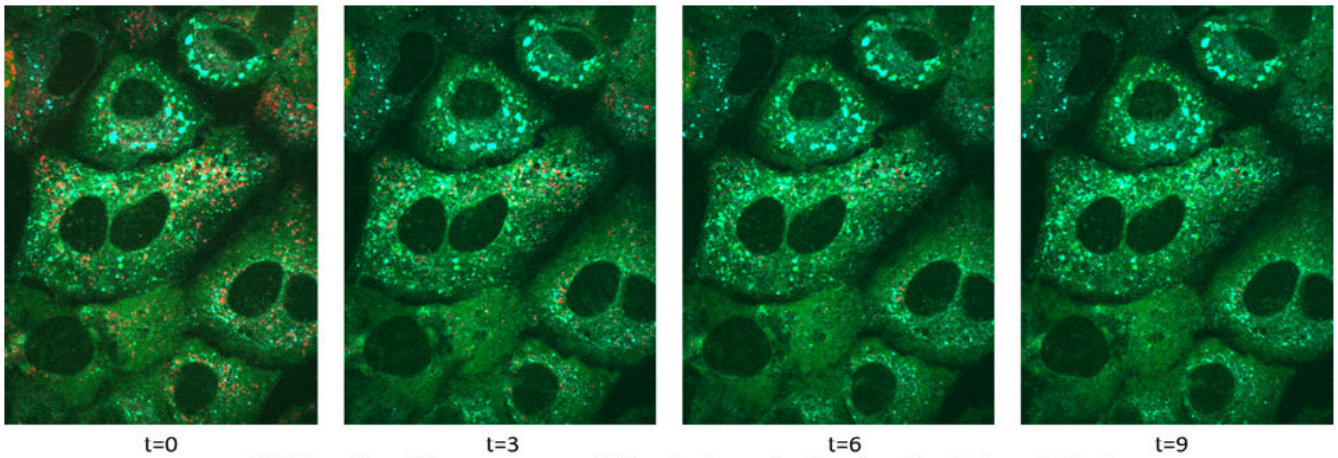

(b) Three-channel image sequence with linearly decreasing intensity values in channel 1 (red).

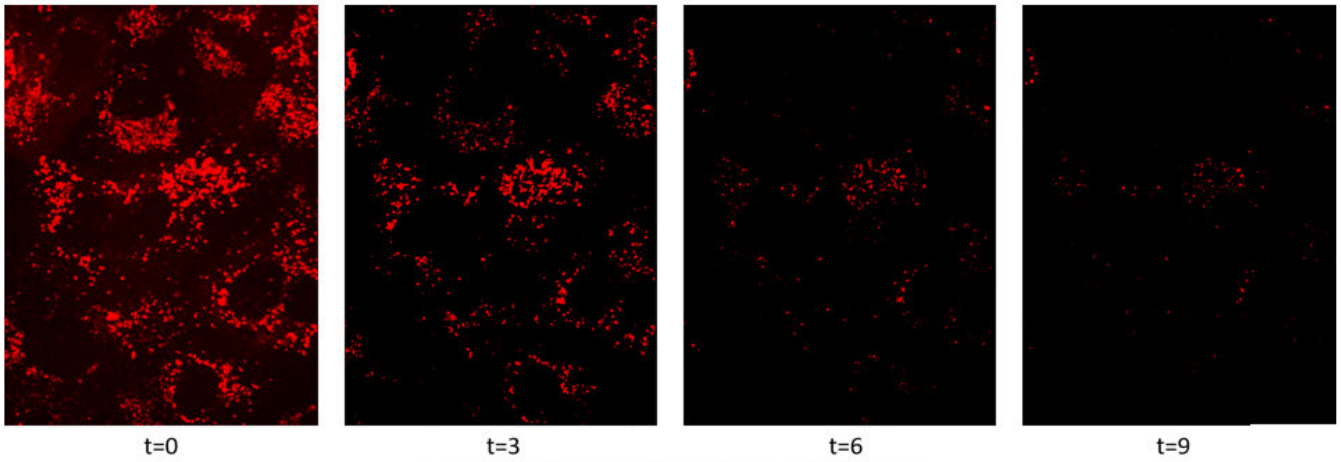

(c) Channel 1 with linearly decreasing intensity values.

FIGURE 8. **Live cell fluorescence microscopy data of HCV proteins. a) Original composite image sequence. b) Composite image sequence with decreasing channel 1 intensity values over time. c) Decreasing channel 1 intensity values over time.**

intuitive visualization of the color composition by a Maxwell color triangle (triple colocalization) or a color ribbon (double colocalization) as well as global statistics of the object intensity, object size, and number of colocalizations over time.

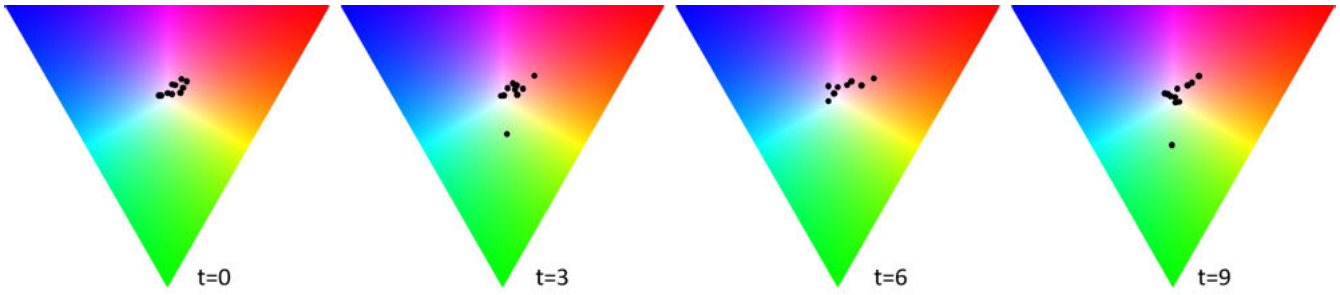

(a) Original image sequence at different time points.

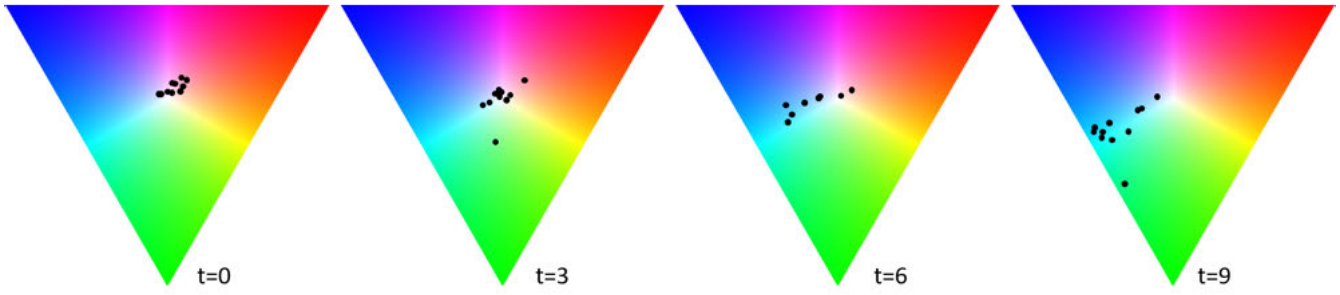

(b) Image sequence with decreasing intensity values in channel 1 (red).

FIGURE 9. Maxwell color triangles for a live cell fluorescence microscopy image sequence of HCV proteins. a) Original image sequence. b) Image sequence with decreasing intensity values for channel 1 over time.

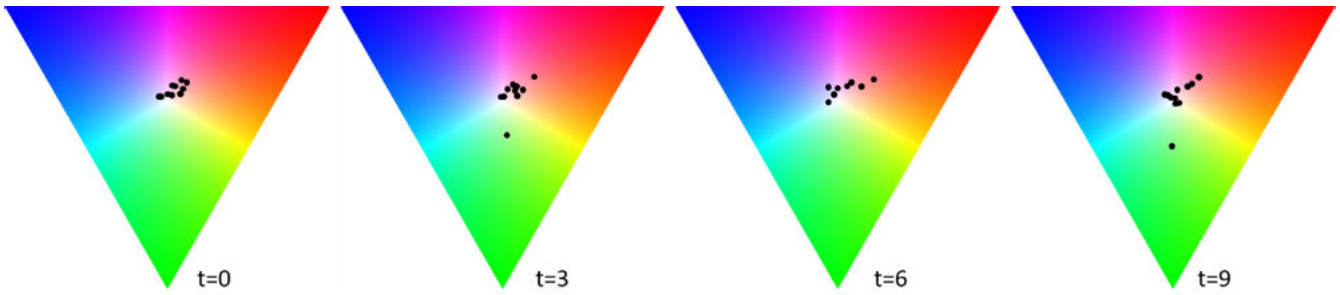

(a) Original image sequence at different time points.

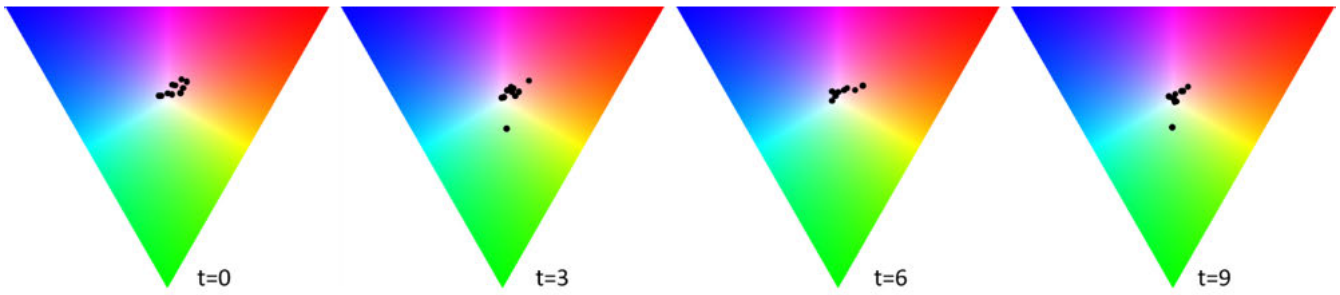

(b) Image sequence with increasing intensity values in all channels.

FIGURE 10. Maxwell color triangles for a live cell fluorescence microscopy image sequence of HCV proteins. a) Original image sequence. b) Image sequence with increasing intensity values in all channels over time.

While the global statistics represent information of individual channels, the object-based color analysis by the Maxwell color triangle or the color ribbon provides combined information of multiple channels. Thus, different aspects of the

image data are represented which complement each other. ColocQuant and ColocJ are efficient and easy to use without requiring programming experience. Obtained quantitative results can be exported to other software for further analysis. We illustrated the application of ColocQuant and ColocJ using multi-channel live cell microscopy images of HCV proteins expressed in virus-replicating cells. We demonstrated the color composition analysis of ColocJ for double and triple colocalization and also presented the visualization of particle positions and distances between the different channels based on the identified colocalizations by ColocQuant. Further, we provided insights on the Maxwell color triangle visualization of triple colocalizations for different image intensity changes typically occurring in fluorescence microscopy image data.

APPENDIX A
MAXWELL COLOR TRIANGLE: MATHEMATICAL ANALYSIS OF INTENSITY CHANGES

For an intensity change (increase or decrease) in one channel of a three-channel image, we show that the position within the Maxwell color triangle generally (i) changes for a linear intensity change, (ii) changes for a non-linear intensity change, and (iii) shifts towards a vertex of the Maxwell color triangle for a linear and non-linear intensity increase. In addition, we show for an intensity change in all three image channels, that the position within the Maxwell color triangle generally (iv) changes for a linear intensity change, (v) is invariant against a non-linear intensity change, and (vi) shifts towards the center of the Maxwell color triangle for a linear intensity change.

A. INTENSITY CHANGE IN ONE IMAGE CHANNEL

We assume that the intensities of the three image channels are $R, G, B > 0$. To proof (i), we consider the case that all intensities of one channel (e.g., red channel) are changed by an additive value $\beta \in \mathbb{R}$ (with $\beta \neq 0$). Doing this for successive time points represents a linear intensity change over time. The intensity values of the other two channels remain unchanged. The position within the Maxwell color triangle does not change if the ratio for the red channel fullfills:

$$\frac{R}{R+G+B} = \frac{R+\beta}{R+\beta+G+B} \tag{1}$$

$$\beta\ (G+B) = 0 \tag{2}$$

However, this is only fullfilled if either $\beta = 0$ or $G+B=0$, which contradicts the assumption. Thus, the position in the Maxwell color triangle changes. To proof (ii), we consider the case that all intensities of one channel (e.g., red channel) are multiplied by a constant factor β (with $\beta \neq 1$). Doing this for successive time points represents a non-linear intensity change. The position within the Maxwell color triangle does not change if the ratio for the red channel fullfills:

$$\frac{R}{R+G+B} = \frac{R\cdot\beta}{R\cdot\beta+G+B} \tag{3}$$

$$\beta\ (G+B) = G+B \tag{4}$$

However, this is only fullfilled if either $\beta = 1$ or $G+B=0$, which contradicts the assumption. Thus, the position in the Maxwell color triangle changes. To proof (iii), we consider the case that all intensities of one channel (e.g., red channel) are changed linearly or non-linearly with β. If β increases towards infinity, the ratio for the red channel approaches 1:

$$\lim_{\beta->\infty}\left(\frac{R+\beta}{R+\beta+G+B}\right) = 1 \tag{5}$$

$$\lim_{\beta->\infty}\left(\frac{R\cdot\beta}{R\cdot\beta+G+B}\right) = 1 \tag{6}$$

The ratio for the remaining channels approaches 0 (e.g., green channel):

$$\lim_{\beta->\infty}\left(\frac{G}{R+\beta+G+B}\right) = 0 \tag{7}$$

$$\lim_{\beta->\infty}\left(\frac{G}{R\cdot\beta+G+B}\right) = 0 \tag{8}$$

A ratio of 1 for one of the three channels (and 0 for the remaining channels) is represented by a vertex of the Maxwell color triangle.

B. INTENSITY CHANGE IN ALL IMAGE CHANNELS

We assume that $R \neq G \neq B$ and $R, G, B > 0$. To proof (iv), we consider the case that all intensities of all three channels are changed linearly with β. The RGB color values within the Maxwell color triangle fullfill:

$$\frac{R}{R+G+B} + \frac{G}{R+G+B} + \frac{B}{R+G+B} = 1 \tag{9}$$

The position within the Maxwell color triangle does not change if the ratio for the red channel fullfills:

$$\frac{R}{R+G+B} = \frac{R+\beta}{R+\beta+G+\beta+B+\beta} \tag{10}$$

$$R = \frac{1}{2}(G+B) \tag{11}$$

Analogously, for the green channel we have $G = \frac{1}{2}(R+B)$ and for the blue channel $B = \frac{1}{2}(R+G)$. However, all three equations are only simultaneously fullfilled if $R = G = B$, which contradicts the assumption. Thus, the position in the Maxwell color triangle changes. For proofing (v), the intensity values in the original image sequence in all three channels are changed non-linearly with β. Since

$$\frac{R\cdot\beta}{R\cdot\beta+G\cdot\beta+B\cdot\beta} = \frac{R}{R+G+B} \tag{12}$$

the position within the Maxwell color triangle does not change and thus is invariant. To proof (vi), we consider the case that all intensities of all three channels are changed linearly with β. If β increases towards infinity, the ratio for each channel goes towards 1/3 (e.g., red channel):

$$\lim_{\beta->\infty}\left(\frac{R+\beta}{R+G+B+3\,\beta}\right) = \frac{1}{3} \tag{13}$$

A ratio of 1/3 for each of the three channels is represented by the center of the Maxwell color triangle. For a non-linear intensity change in all channels, if β increases towards infinity, the ratio does not change, as shown above in (v).

ACKNOWLEDGMENT

(Christian Ritter and Roman Thielemann contributed equally to this work.)

REFERENCES

[1] K.-S. Chang, J. Jiang, Z. Cai, and G. Luo, "Human apolipoprotein E is required for infectivity and production of hepatitis C virus in cell culture," *J. Virol.*, vol. 81, no. 24, pp. 13783–13793, Dec. 2007.

[2] J.-Y. Lee, M. Cortese, U. Haselmann, K. Tabata, I. Romero-Brey, C. Funaya, N. L. Schieber, Y. Qiang, M. Bartenschlager, S. Kallis, C. Ritter, K. Rohr, Y. Schwab, A. Ruggieri, and R. Bartenschlager, "Spatiotemporal coupling of the hepatitis C virus replication cycle by creating a lipid droplet-proximal membranous replication compartment," *Cell Rep.*, vol. 27, no. 12, pp. 3602.e5–3617.e5, Jun. 2019.

[3] L. P. Nguyen, T. T. T. Nguyen, H. C. Nguyen, H. T. Pham, K. M. Han, D. H. Choi, E.-M. Park, S. M. Kang, D. Tark, Y.-S. Lim, and S. B. Hwang, "Cortactin interacts with hepatitis c virus core and NS5A proteins: Implications for virion assembly," *J. Virol.*, vol. 94, no. 19, pp. 1–18, Sep. 2020.

[4] S. Bolte and F. P. Cordelières, "A guided tour into subcellular colocalization analysis in light microscopy," *J. Microsc.*, vol. 224, no. 3, pp. 213–232, Dec. 2006.

[5] K. W. Dunn, M. M. Kamocka, and J. H. McDonald, "A practical guide to evaluating colocalization in biological microscopy," *Amer. J. Physiol.-Cell Physiol.*, vol. 300, no. 4, pp. C723–C742, Apr. 2011.

[6] T. Lagache, N. Sauvonnet, L. Danglot, and J.-C. Olivo-Marin, "Statistical analysis of molecule colocalization in bioimaging," *Cytometry A*, vol. 87, no. 6, pp. 568–579, Jun. 2015.

[7] E. M. Manders, J. Stap, G. J. Brakenhoff, R. van Driel, and J. A. Aten, "Dynamics of three-dimensional replication patterns during the S-phase, analysed by double labelling of DNA and confocal microscopy," *J. Cell Sci.*, vol. 103, no. 3, pp. 857–862, Nov. 1992.

[8] E. M. M. Manders, F. J. Verbeek, and J. A. Aten, "Measurement of co-localization of objects in dual-colour confocal images," *J. Microsc.*, vol. 169, no. 3, pp. 375–382, Mar. 1993.

[9] B. van Steensel, E. P. van Binnendijk, C. D. Hornsby, H. T. van der Voort, Z. S. Krozowski, E. R. de Kloet, and R. van Driel, "Partial colocalization of glucocorticoid and mineralocorticoid receptors in discrete compartments in nuclei of rat hippocampus neurons," *J. Cell Sci.*, vol. 109, no. 4, pp. 787–792, Apr. 1996.

[10] S. V. Costes, D. Daelemans, E. H. Cho, Z. Dobbin, G. Pavlakis, and S. Lockett, "Automatic and quantitative measurement of protein-protein colocalization in live cells," *Biophys. J.*, vol. 86, no. 6, pp. 3993–4003, Jun. 2004.

[11] Q. Li, A. Lau, T. J. Morris, L. Guo, C. B. Fordyce, and E. F. Stanley, "A syntaxin 1, Gα_0, and N-type calcium channel complex at a presynaptic nerve terminal: Analysis by quantitative immunocolocalization," *J. Neurosci.*, vol. 24, no. 16, pp. 4070–4081, 2004.

[12] H. Sheng, W. Stauffer, and H. N. Lim, "Systematic and general method for quantifying localization in microscopy images," *Biol. Open*, vol. 5, no. 12, pp. 1882–1893, Dec. 2016.

[13] E. Lachmanovich, D. E. Shvartsman, Y. Malka, C. Botvin, Y. I. Henis, and A. M. Weiss, "Co-localization analysis of complex formation among membrane proteins by computerized fluorescence microscopy: Application to immunofluorescence co-patching studies," *J. Microsc.*, vol. 212, no. 2, pp. 122–131, Nov. 2003.

[14] F. Jaskolski, C. Mulle, and O. J. Manzoni, "An automated method to quantify and visualize colocalized fluorescent signals," *J. Neurosci. Methods*, vol. 146, no. 1, pp. 42–49, Jul. 2005.

[15] Y. Boutté, M.-T. Crosnier, N. Carraro, J. Traas, and B. Satiat-Jeunemaitre, "The plasma membrane recycling pathway and cell polarity in plants: Studies on PIN proteins," *J. Cell Sci.*, vol. 119, no. 7, pp. 1255–1265, Apr. 2006.

[16] B. Zhang, N. Chenouard, J.-C. Olivo-Marin, and V. Meas-Yedid, "Statistical colocalization in biological imaging with false discovery control," in *Proc. 5th IEEE Int. Symp. Biomed. Imag., From Nano Macro*, May 2008, pp. 1327–1330.

[17] J. A. Helmuth, G. Paul, and I. F. Sbalzarini, "Beyond co-localization: Inferring spatial interactions between sub-cellular structures from microscopy images," *BMC Bioinf.*, vol. 11, no. 1, pp. 1–12, Dec. 2010.

[18] S. Wörz, P. Sander, M. Pfannmoller, R. J. Rieker, S. Joos, G. Mechtersheimer, P. Boukamp, P. Lichter, and K. Rohr, "3D geometry-based quantification of colocalizations in multichannel 3D microscopy images of human soft tissue tumors," *IEEE Trans. Med. Imag.*, vol. 29, no. 8, pp. 1474–1484, Aug. 2010.

[19] T. Lagache, V. Meas-Yedid, and J.-C. Olivo-Marin, "A statistical analysis of spatial colocalization using Ripley's k function," in *Proc. IEEE 10th Int. Symp. Biomed. Imag.*, Apr. 2013, pp. 896–901.

[20] A. Dupont, K. Stirnnagel, D. Lindemann, and D. C. Lamb, "Tracking image correlation: Combining single-particle tracking and image correlation," *Biophys. J.*, vol. 104, no. 11, pp. 2373–2382, Jun. 2013.

[21] D. Vercauteren, H. Deschout, K. Remaut, J. F. J. Engbersen, A. T. Jones, J. Demeester, S. C. De Smedt, and K. Braeckmans, "Dynamic colocalization microscopy to characterize intracellular trafficking of nanomedicines," *ACS Nano*, vol. 5, no. 10, pp. 7874–7884, Oct. 2011.

[22] H. Deschout, T. Martens, D. Vercauteren, K. Remaut, J. Demeester, S. De Smedt, K. Neyts, and K. Braeckmans, "Correlation of dual colour single particle trajectories for improved detection and analysis of interactions in living cells," *Int. J. Mol. Sci.*, vol. 14, no. 8, pp. 16485–16514, Aug. 2013.

[23] Y. Qiang, J. Y. Lee, R. Bartenschlager, and K. Rohr, "Colocalization analysis and particle tracking in multi-channel fluorescence microscopy images," in *Proc. IEEE 14th Int. Symp. Biomed. Imag. (ISBI)*, Apr. 2017, pp. 646–649.

[24] A. Rizk, G. Paul, P. Incardona, M. Bugarski, M. Mansouri, A. Niemann, U. Ziegler, P. Berger, and I. F. Sbalzarini, "Segmentation and quantification of subcellular structures in fluorescence microscopy images using squassh," *Nature Protocols*, vol. 9, no. 3, pp. 586–596, Mar. 2014.

[25] J.-F. Gilles, M. Dos Santos, T. Boudier, S. Bolte, and N. Heck, "DiAna, an ImageJ tool for object-based 3D co-localization and distance analysis," *Methods*, vol. 115, pp. 55–64, Feb. 2017.

[26] W. Stauffer, H. Sheng, and H. N. Lim, "EzColocalization: An ImageJ plugin for visualizing and measuring colocalization in cells and organisms," *Sci. Rep.*, vol. 8, no. 1, pp. 1–13, Oct. 2018.

[27] A. Gorlewicz, K. Krawczyk, A. A. Szczepankiewicz, P. Trzaskoma, C. Mulle, and G. M. Wilczynski, "Colocalization colormap—An ImageJ plugin for the quantification and visualization of colocalized signals," *Neuroinformatics*, vol. 18, no. 4, pp. 661–664, Oct. 2020.

[28] T. J. Collins, "ImageJ for microscopy," *BioTechniques*, vol. 43, no. 1S, pp. S25–S30, Jul. 2007.

[29] J. L. Bentley, "Multidimensional binary search trees used for associative searching," *Commun. ACM*, vol. 18, no. 9, pp. 509–517, Sep. 1975.

[30] D. Sage, F. R. Neumann, F. Hediger, S. M. Gasser, and M. Unser, "Automatic tracking of individual fluorescence particles: Application to the study of chromosome dynamics," *IEEE Trans. Image Process.*, vol. 14, no. 9, pp. 1372–1383, Sep. 2005.

[31] J. H. Friedman, J. L. Bentley, and R. A. Finkel, "An algorithm for finding best matches in logarithmic expected time," *ACM Trans. Math. Softw.*, vol. 3, no. 3, pp. 209–226, Sep. 1977.

[32] C. Ritter, "Data fusion and Bayesian smoothing for tracking in fluorescence microscopy images," Ph.D. dissertation, Heidelberg Univ., Heidelberg, Germany, 2022.

[33] J. C. Maxwell, "Experiments on colour, as perceived by the eye, with remarks on colour-blindness," *Trans. Roy. Soc. Edinburgh*, vol. 21, pp. 299–301, 1855.

[34] G. Peruzzi and V. Roberti, "The color top and the distinction between additive and subtractive color mixing [historical corner]," *IEEE Antennas Propag. Mag.*, vol. 61, no. 5, pp. 138–145, Oct. 2019.

[35] R. M. Haralick, "Some neighborhood operators," in *Real-Time Parallel Computing*, 1981, pp. 11–35.

[36] S. Ivanchenko, W. J. Godinez, M. Lampe, H.-G. Kräusslich, R. Eils, K. Rohr, C. Bräuchle, B. Müller, and D. C. Lamb, "Dynamics of HIV-1 assembly and release," *PLoS Pathogens*, vol. 5, no. 11, pp. 1–12, 2009.

[37] S. Padilla-Parra, M. Marin, N. Kondo, and G. B. Melikyan, "Pinpointing retrovirus entry sites in cells expressing alternatively spliced receptor isoforms by single virus imaging," *Retrovirology*, vol. 11, no. 1, pp. 1–14, Dec. 2014.
[38] L. Song, E. J. Hennink, I. T. Young, and H. J. Tanke, "Photobleaching kinetics of fluorescein in quantitative fluorescence microscopy," *Biophys. J.*, vol. 68, no. 6, pp. 2588–2600, Jun. 1995.
[39] E. Bakker and P. S. Swain, "Estimating numbers of intracellular molecules through analysing fluctuations in photobleaching," *Sci. Rep.*, vol. 9, no. 1, pp. 1–13, Oct. 2019.
[40] M. T. Pham, J.-Y. Lee, C. Ritter, R. Thielemann, U. Haselmann, C. Funaya, V. Laketa, K. Rohr, and R. Bartenschlager, "Intercellular transmission of viral RNA by Apolipoprotein E associated extracellular vesicles," Tech. Rep., 2022.

CHRISTIAN RITTER received the B.Sc. and M.Sc. degrees in electrical engineering and information technology from the Karlsruhe Institute of Technology (KIT), Germany, in 2013 and 2016, respectively, and the Ph.D. degree in computational science and engineering from Heidelberg University, Germany, in 2022. His research interests include the development of methods for detecting, tracking, and analyzing objects in live cell microscopy image sequences.

ROMAN THIELEMANN received the M.Sc. degree in molecular biotechnology with a major in bioinformatics from Heidelberg University, Germany, in 2021. He is currently pursuing the Ph.D. degree with the NNF Center for Basic Metabolic Research, Copenhagen, Denmark. His research interest includes the use of machine learning methods to integrate various data types in the context of diabetes.

JI-YOUNG LEE received the master's degree in interdisciplinary program with brain science from Seoul National University, South Korea, in 2007, and the Ph.D. degree in molecular virology from Heidelberg University, Germany, in 2014. From 2007 to 2009, she was with the Institut Pasteur Korea, South Korea, as a Researcher. Since 2014, she has been a Postdoctoral Researcher with the Department of Infectious Diseases, Heidelberg University, to investigate the Hepatitis C virus assembly process.

MINH TU PHAM received the master's degree in biomedical gerontology with the focus on the Hepatitis C virus from Hallym University, South Korea, in 2016, and the Ph.D. degree in molecular virology from Heidelberg University, Germany, in 2022. His research interests include light and electron microscopic methods to visualize the host and viral proteins in nave and virus-infected cells aiming to understand the basic cellular and viral biology.

RALF BARTENSCHLAGER received the Ph.D. degree in biology from Heidelberg University, Germany, in 1990. After a Postdoctoral Researcher stay in industry until 1993, he joined the University of Mainz, Germany, to establish his independent research group. In 2003, he joined Heidelberg University to establish the Research Division Molecular Virology with the Center for Infectious Diseases. His work centers on flavi-hepatitis and corona viruses, studying the cell biology underlying productive virus replication, how these viruses escape innate immunity, and the development of antiviral drugs.

KARL ROHR received the Dipl.-Ing. degree in electrical engineering from the University of Karlsruhe (KIT), Germany, and the Ph.D. and Habilitation degrees in computer science from the University of Hamburg, Germany, in 1994 and 1999, respectively.

From 2000 to 2004, he was an Associate Professor with the International University, Germany. In 1999, he spent a research stay with the Surgical Planning Laboratory, Harvard Medical School, Boston, MA, USA. He is currently an Associate Professor and the Head of the Biomedical Computer Vision Group (BMCV), Heidelberg University. He has written a book titled *Landmark-Based Image Analysis* (Kluwer Academic Publishers, 2001) and published more than 300 peer-reviewed scientific articles. His research interests include biomedical image analysis with focus on cell segmentation, particle and cell tracking, non-rigid image registration, vessel segmentation, and landmark localization.

Prof. Rohr was the Program Chair of the IEEE International Symposium on Biomedical Imaging (ISBI), in 2016. He was an Associate Editor of IEEE TRANSACTIONS ON BIOMEDICAL ENGINEERING, from 2007 to 2012, and served the editorial board for the journal *Pattern Recognition*, from 2000 to 2006.